Strain-Controlled Superconductivity in Few-Layer NbSe$_2$

Cliff Chen, Protik Das, Ece Aytan, Weimin Zhou, Justin Horowitz, Biswarup Satpati, Alexander A. Balandin, Roger K. Lake, and Peng Wei*

Read Online

ACCESS | Metrics & More | Article Recommendations | Supporting Information

ABSTRACT: The controlled tunability of superconductivity in low-dimensional materials may enable new quantum devices. Particularly in triplet or topological superconductors, tunneling devices such as Josephson junctions, etc., can demonstrate exotic functionalities. The tunnel barrier, an insulating or normal material layer separating two superconductors, is a key component for the junctions. Thin layers of NbSe$_2$ have been shown as a superconductor with strong spin orbit coupling, which can give rise to topological superconductivity if driven by a large magnetic exchange field. Here we demonstrate the superconductor−insulator transitions in epitaxially grown few-layer NbSe$_2$ with wafer-scale uniformity on insulating substrates. We provide the electrical transport, Raman spectroscopy, cross-sectional transmission electron microscopy, and X-ray diffraction characterizations of the insulating phase. We show that the superconductor−insulator transition is driven by strain, which also causes characteristic energy shifts of the Raman modes. Our observation paves the way for high-quality heterojunction tunnel barriers to be seamlessly built into epitaxial NbSe$_2$ itself, thereby enabling highly scalable tunneling devices for superconductor-based quantum electronics.

KEYWORDS: two-dimensional material, tunable superconductor, heterostructure material, strain effect at interface, superconducting devices

1. INTRODUCTION

Imposing structural perturbations to thin layers of NbSe$_2$ can be used as a potential knob to control superconductivity. NbSe$_2$ is often found in its prismatic 2H phase, i.e., the superconducting phase, in devices fabricated from exfoliated thin crystals.[1,3,9] Insulating NbSe$_2$ is rare,[10] although it has been recently demonstrated in the 1T phase of NbSe$_2$.[11] However, a controlled tuning in between the superconducting and insulating states of NbSe$_2$ has not yet been achieved. NbSe$_2$ thin layers are often either exfoliated or grown on another two-dimensional (2D) material such as graphene.[2,12] Because of the van der Waals interaction, the coupling between the layer and the substrate is weak, and the substrate often does not play a major role in determining the electrical properties of NbSe$_2$.

2. EXPERIMENTAL METHODS AND RESULTS

We demonstrate the electrical properties of few-layer NbSe$_2$ grown using MBE on a non 2D material substrate, i.e., on sapphire. Because the growth is epitaxial, the sapphire substrate couples to the NbSe$_2$ layer. One evidence of such coupling is seen from the locked [210] crystalline directions between the substrate and the NbSe$_2$ layer as observed in situ by reflection high energy electron diffraction (RHEED) during the growth (Figure 1c). Ideally, NbSe$_2$ has a much smaller lattice constant ($a \approx 3.44$ Å)[13] compared to that of the c-cut sapphire ($a \approx 4.76$ Å), and one would not expect the growth to
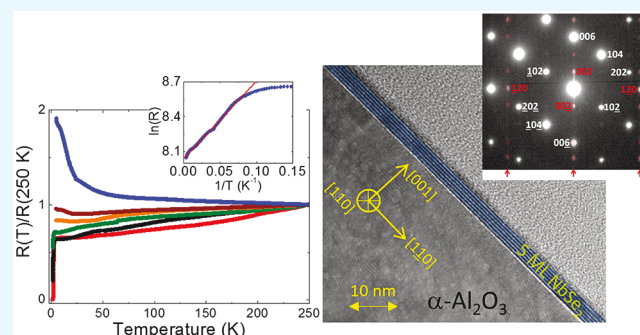
be epitaxial. However, by considering the 3 × 3 unit cells of NbSe$_2$ and the 2 × 2 unit cells of the c-cut sapphires surface, the two crystals do match with each other and the mismatch is only ∼7.8%. Such superlattice cell matching has been previously reported in the epitaxial growth of high-quality transition-metal dichalcogenides (TMD) thin layers, for example, WSe$_2$, on sapphire substrate.[14] Notably, when considering the superlattice matching, the c-cut sapphire substrate imposes a planar compressive strain to NbSe$_2$. Similar heterogeneous growth, i.e., growing a material epitaxially on top of another one with drastically different properties has demonstrated many emerging physics phenomena. One example is the epitaxial growth of Fe on GaAs(001) giving rise to the Fe/GaAs(001) heterostructures, in which tunneling anisotropic magnetoresistance and spin−orbit proximity effects have been shown.[15,16]

By controlling the growth temperatures, we obtain the NbSe$_2$ layers with two distinctive phases: one being a superconductor and the other one being an insulator (or semiconductor). Because our substrate is sapphire, we are able to carry out the electrical transport characterizations of both phases. We confirm that the insulating (or semiconducting) NbSe$_2$ has a gapped Fermi surface and demonstrates
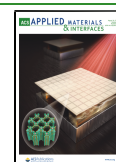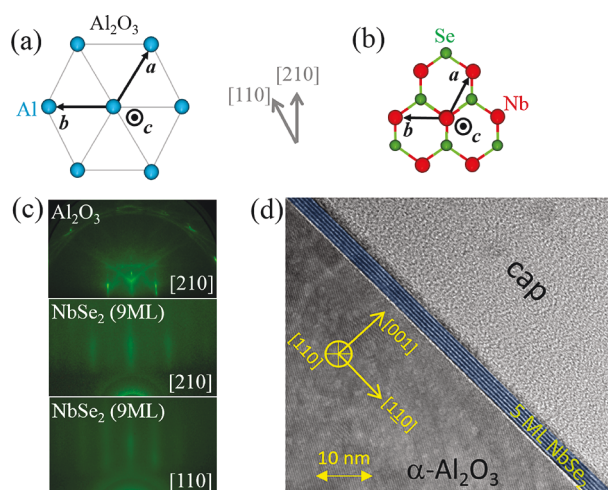
Figure 1. (a) Schematic showing the Al atoms on sapphire (0001) surface. (b) Schematic of $NbSe_2$ surface and its epitaxial orientation with respect to the substrate in a. (c) RHEED patterns: sapphire substrate along the [210] direction (top), 9 ML $NbSe_2$ along the [210] direction (middle), and along the [110] direction (bottom). (d) TEM image of a 5 ML $NbSe_2$ sample. It can be clearly seen that each $NbSe_2$ monolayer extends continuously over a large scale.

a shift of the Raman peaks with respect to the standard 2H-$NbSe_2$ Raman modes. It is known that the Raman peak shift often indicates a hardening or softening of the lattice vibration modes, which may result from lattice strain effect. Using selective area diffraction (SAD) based on cross-sectional transmission electron microscopy (TEM) and X-ray diffraction (XRD), we show a lateral compression and a vertical expansion of the $NbSe_2$ lattice, agreeing well with the Raman results. Our findings provide insight into the transition between the insulating and superconducting electronic properties of the two phases.

The quality of our epitaxially grown $NbSe_2$, including crystal symmetry and epitaxial orientation, is confirmed by in situ RHEED experiment (Figure 1a−c). A 0.5 monolayer (ML) $NbSe_2$ seed, which does not completely cover the sapphire substrate, is used to facilitate the growth (see the Supporting Information). The 6-fold rotational symmetry of the grown layer is confirmed by a planar rotation of the RHEED electron beam from [210] to [110] directions (Figure 1c). It is also clear that the crystalline orientations of $NbSe_2$ and sapphire are locked as $[210]_{NbSe2}$ // $[210]_{sapphire}$ (Figure 1a−c), which infers that there is an interaction between $NbSe_2$ and the substrate and thus would lead to strain effect.

The growth is proved to be layer-by-layer. Each monolayer of $NbSe_2$ is clearly defined as shown in the TEM image (Figure 1d, 5 ML $NbSe_2$). According to the scale bar of the TEM image, Figure 1d also shows that each $NbSe_2$ monolayer extends continuously over a large distance. It thus suggests that atomically thin $NbSe_2$ on sapphire
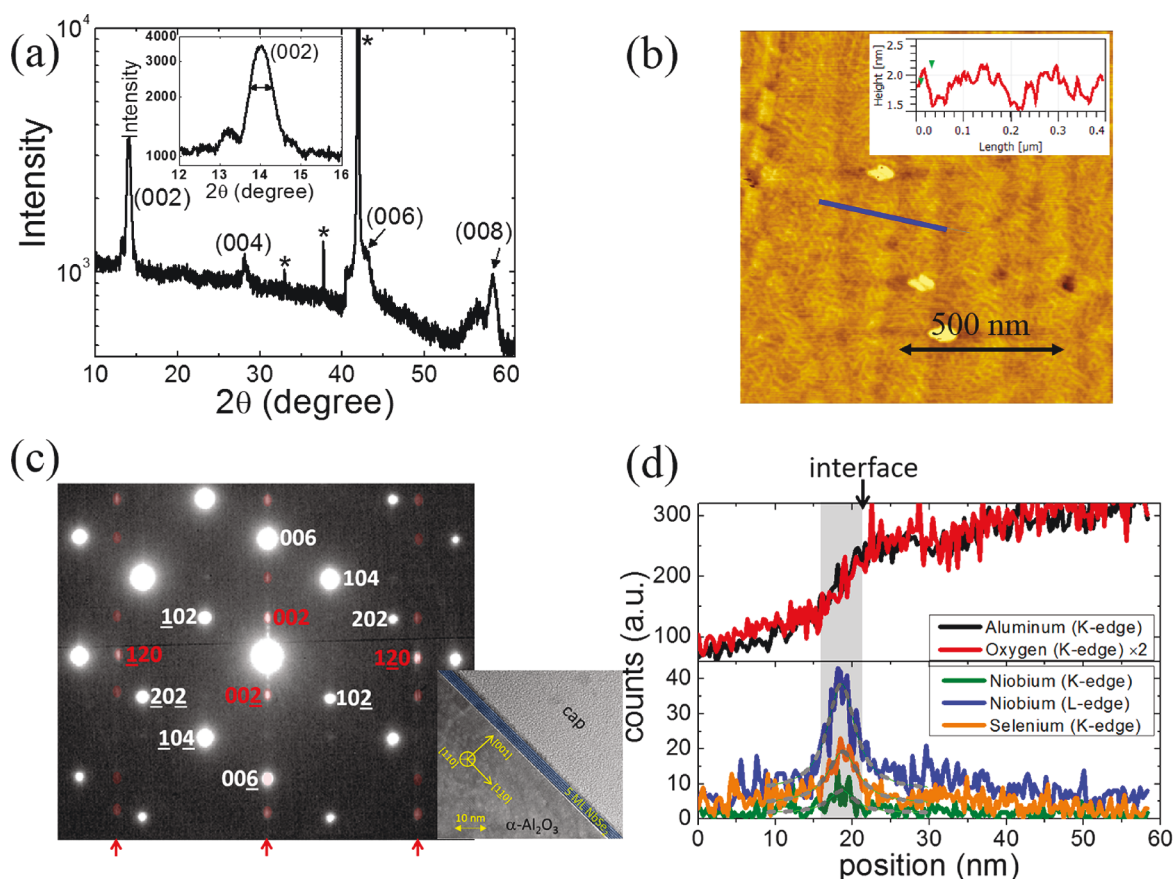

Figure 2. (a) X-ray diffraction of a $NbSe_2$ sample. The well-oriented *c*-axis diffraction peaks are seen. The starred peaks correspond to the substrate and the background from the instrument. The inset provides a magnified image of the (002) peak, which also shows signatures of thickness fringes. (b) AFM image of a continuous (island-free) 3 ML $NbSe_2$ sample following the growth procedure shown in the Supporting Information. The substrate terraces are visible indicating good surface coverage. (c) TEM based selective area diffraction (SAD) data of the 5 ML $NbSe_2$ sample (inset). The substrate diffraction peaks are labeled in white and the $NbSe_2$ diffraction peaks are in red. The *c*-axis (002) diffraction of $NbSe_2$ is aligned with the *c*-axis (006) diffraction of sapphire. (d) Element-selective spatially resolved energy-dispersive X-ray spectroscopy (EDX) data of a line across the interface of the layer. The data show no element segregations in the layer and a clear interface with the substrate. The stoichiometric ratio between Nb and Se is determined in Supporting Information Figure S2b.
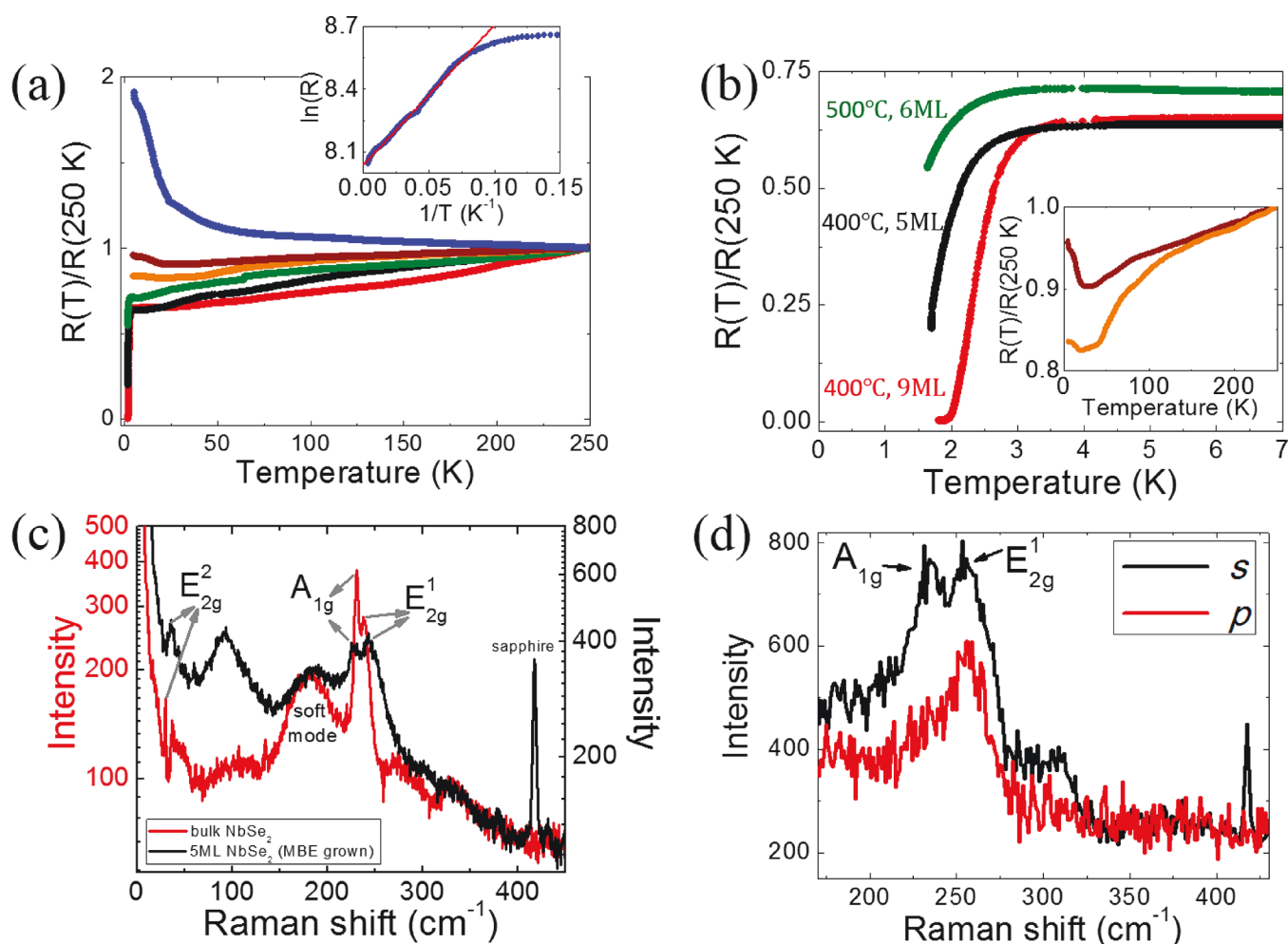
Figure 3. (a) Resistance measurements of the superconductor to insulator transition in $NbSe_2$ samples systematically tuned by varying the growth temperature (from 400 to 600 °C). Inset: the $\ln(R)$ vs $1/T$ plot of the insulating sample. The linear fit works in the full temperature range from 13 K and above, which gives an excitation gap $\frac{E_0}{k_B} \approx 6.7$ K. (b) Low-temperature zoomed-in plot of the superconducting samples. Inset: the metallic samples demonstrating low temperature insulating behavior. The color of each curve matches that of a. (c) Raman spectra comparison between MBE grown superconducting $NbSe_2$ (black) and a bulk sample (red). The MBE-grown sample has a blue shift for E^1_{2g} and a red shift for A_{1g}. (d) Polarized Raman spectroscopy confirming both the A_{1g} and E^1_{2g} Raman modes of the sample shown in the middle panel of Figure 4a. The A_{1g} is turned off when switching from s- to p-polarization, whereas the E^1_{2g} peak survives.

is achievable using MBE. The wafer-scale coverage of $NbSe_2$ is further confirmed by both XRD and atomic force microscopy (AFM) (Figure 2a, b). The quality of $NbSe_2$ is demonstrated by a set of characteristic XRD diffraction peaks (Figure 2a). AFM shows that the grown $NbSe_2$ layer has a wafer-scale coverage over the substrate (Figure 2b). The terrace-like feature in Figure 2b indicates that the $NbSe_2$ layer follows the atomic terraces of sapphire, which agrees with the uniform island-free growth of $NbSe_2$. The crystalline quality of the $NbSe_2$ samples, down to a few MLs, is also confirmed by electron diffractions carried out locally in a cross-sectional region of $NbSe_2$ using SAD (Figure 2c). The $NbSe_2$ diffraction pattern is distinct from the substrate pattern with the (002) series diffraction spots aligned with the (006) series of the sapphire substrate. The spatially resolved energy-dispersive X-ray spectroscopy (EDX) line scan shows no element segregations in the layer and a clear interface with the substrate. The EDX also shows no contamination in the $NbSe_2$ layer, and an atomic ratio ~1:2 for Nb:Se (Supporting Information Figure S2b). Further, using atomically resolved scanning transmission electron microscopy (STEM), the relative arrangement of Nb and Se atoms is clearly observed (Supporting Information Figure S1c). The above studies confirm that stochiometric $NbSe_2$ layers have been grown.

A systematic tuning of the superconductivity is achieved by controlling the growth condition of in $NbSe_2$ (Figure 3a). Both

increasing the growth temperature and decreasing the layer thickness cause a decrease of T_C (Figure 3b). However, as the growth temperature increases, even in thick samples, the sample resistance starts to develop a sharp upturn at low temperature (Figure 3b inset). To clarify the origin of the resistance upturn, we increase the growth temperature to 600 °C, which gives rise to an insulating (or semiconducting) $NbSe_2$ sample in the full temperature range (Figure 3a blue). A plot of $\ln(R)$ vs T^{-1} is used to validate the origin of the insulating behavior. We find that a linear fit well describes the $\ln(R)$ vs T^{-1} plot (Figure 3a inset) in a wide temperature range (13 K and above), which is not the case if a variable range hopping model is adopted (Supporting Information Figure S4). Thus, the insulating behavior is not due to localization effects caused by defects. It confirms a gapped Fermi surface with the conductivity given by $\sigma \approx e^{-E_0/k_B T}$, where the activation energy determined to be $\frac{E_0}{k_B} \approx 6.7$

K. Interestingly, we see little changes on crystal structure between the superconducting and insulating samples (Supporting Information Figure S2a). Both have similar lattice constants and the same hexagonal rotation symmetry (Supporting Information Figure S2a). Further, the insulating sample (grown at $T_g \approx 600$ °C) has even better sample quality (Supporting Information Figures S2a and S3).

Therefore, the insulating behavior is not due to the degradation of the $NbSe_2$ sample when growing at 600 °C.

Although RHEED does not show visible changes, the difference between the two types of $NbSe_2$ samples is visible in Raman spectroscopy, which is known to be sensitive to various structural transitions in a wide range of materials.[17,18] First, we compare the Raman spectrum of a 5 ML superconducting sample to that of a bulk $NbSe_2$ flake in Figure 3c. The two spectra resemble each other by both showing the A_{1g}, E^1_{2g}, and soft mode peaks, which confirms the quality of the MBE-grown layer. Compared to bulk $NbSe_2$, it is clear that the E^1_{2g} peak of the MBE-grown $NbSe_2$ blue shifts to a higher wavenumber, whereas the A_{1g} peak red shifts to a lower wavenumber (Figure 3c). The nature of the E^1_{2g} and A_{1g} vibration modes is further confirmed by polarized Raman spectroscopy (Figure 3d), in which the p-polarization turns off the A_{1g} peak while maintaining the E^1_{2g} peak, consistent with prior reports in $2H-NbSe_2$.[9] The blue shift of E^1_{2g} or the red shift of A_{1g} is related to the hardening or softening of phonons, which could be a result of the change in lattice parameters due to strain.[19] It is also known that the hardening of a phonon mode is often unfavorable to superconductivity.

To further understand the change in the Raman modes, we carried out a series of Raman spectroscopy experiments with a focus on the shift of the E^1_{2g} and A_{1g} peaks (Figure 4a). The measurement is done in a set of $NbSe_2$ samples (ranging from superconducting to insulating) that are grown at difference temperatures. The corresponding resistance as a function of temperature is plotted in Figure 3a. A two-peak Gaussian fit is adopted to identify the E^1_{2g} and A_{1g} peak locations (Figure 4a). A clear increase in the E^1_{2g} peak, from 245 to 260 cm^{-1}, is observed, which corresponds to the transition from superconducting to insulating in $NbSe_2$. At the same time, the A_{1g} peak decreases slightly. The validity of the comparison is guaranteed by the aligned sapphire substrate Raman peak at 418 cm^{-1}. It has been shown that the E^1_{2g} mode represents the vibration of atoms within a monolayer layer of $NbSe_2$, and the A_{1g} mode represents the vibration perpendicular to the monolayer.[20] The opposite shift of the E^1_{2g} and A_{1g} modes could reflect different strain effects parallel and perpendicular to the monolayer. Because the (001) plane of $NbSe_2$ is in parallel to the (001) plane of sapphire, the shift in E^1_{2g} could be due to the strain effect within the $NbSe_2$ monolayer. To confirm it, we carried out SAD in both the superconducting sample (growth temperature $T_g \approx 400$ °C) and the insulating sample (growth temperature $T_g \approx 600$ °C). Figure 4b shows a result of the comparison of SAD. There is a clear shift of the $NbSe_2$ (122) SAD diffraction spot. The validity of the comparison is based on the well-aligned $NbSe_2$ (002) and Al_2O_3 (102) SAD diffraction spots by knowing that the $NbSe_2$ (002) spot is along the same direction as the Al_2O_3 (006) spot (Figure 2c). Comparing the insulating sample ($T_g \approx 600$ °C) with the superconducting sample ($T_g \approx 400$ °C), one can see that the $NbSe_2$ (122) SAD spot moves away in the k-space, which indicates a planar compression of the crystal lattice for the insulating sample.

Furthermore, to accurately determine the change of lattice constants along the c-axis direction, we carried out XRD measurements on both types of samples (Figure 4c). After aligning the Al_2O_3 (006) peaks, one can see that the insulating sample ($T_g \approx 600$ °C) has a lower $NbSe_2$ (002) peak, which proves the increased (or expanded) c-axis lattice constant. The planar compression and out-of-plane expansion of the crystal lattice agrees with the Raman results, in which the E^1_{2g} has a blue shift and A_{1g} has a red shift (Figure 4a). The planar lattice compression also agrees with the aforementioned lattice mismatch between $NbSe_2$ and the sapphire substrate when considering the 7.8% smaller sapphire supercell compared to that of $NbSe_2$, which has also been shown in the MBE growth of other TMD materials on sapphire.[14] On the other hand, the compression of the planar crystal lattice could also result in an increase in the c-axis lattice constant causing a red shift to the A_{1g} mode that describes the out-of-plane lattice vibrations.
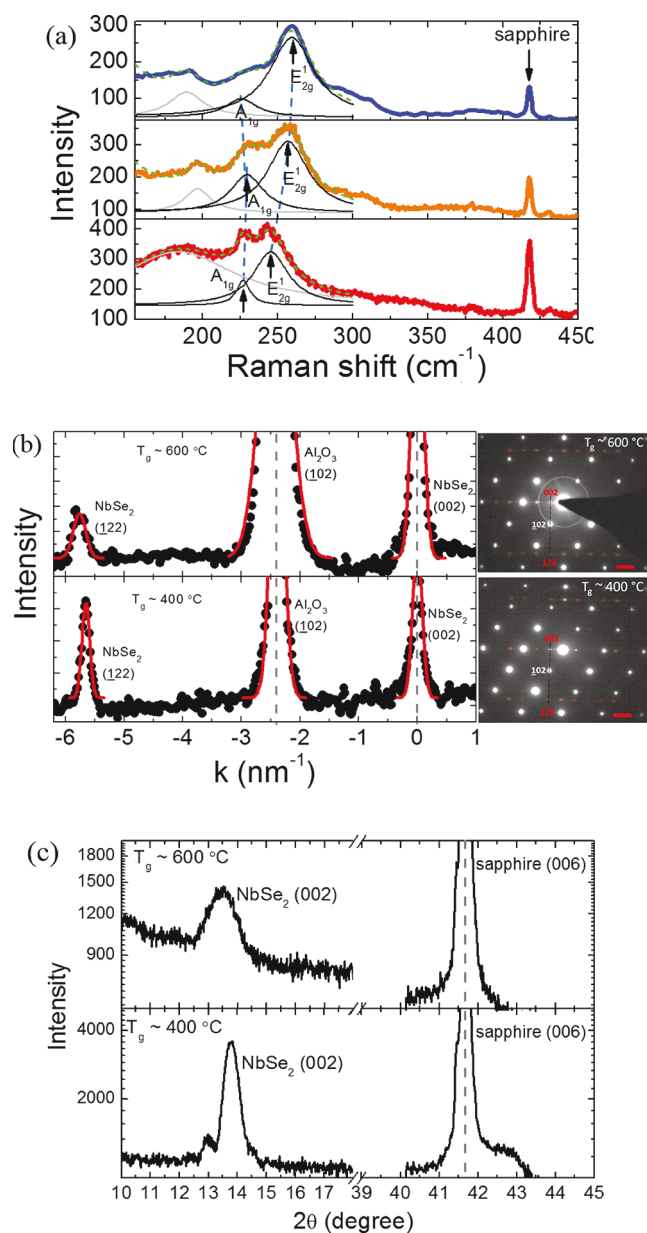

Figure 4. (a) Comparison of the Raman spectra among three samples having different electrical properties (the superconducting sample, the insulating sample, and a sample in between). The color of the data matches that in Figure 3a. Two-peak Gaussian fit (dashed line) is used to identify the locations of the E^1_{2g} and A_{1g} peaks. A red shift of the A_{1g} peak and a blue shift of the E^1_{2g} peak are observed, which accompanies the loss of superconductivity. The comparison is guaranteed by the aligned sapphire peak. (b) The comparison of the SAD results of two samples grown at $T_g \approx 600$ °C (top, insulating) and at $T_g \approx 400$ °C (bottom, superconducting), respectively. A line cut is made from the $NbSe_2$ SAD (002) peak to the NbSe2 SAD (122) peak crossing the sapphire SAD (102) peak. The line cut is indicated by the dashed line shown in the TEM images (right). Gaussian fit is used to identify the locations of the diffraction peaks. By aligning the $NbSe_2$ (002) and sapphire (102) peaks (left), one can see a clear shift of the $NbSe_2$ (122) peak indicating that the sample grown at $T_g \approx 600$ °C has a slightly smaller lattice constant. (c) XRD results of two samples grown at $T_g \approx 600$ °C (top) and at $T_g \approx 400$ °C (bottom). The $NbSe_2$ (002) XRD peak shifts to lower angel for the sample grown at $T_g \approx 600$ °C suggesting an expanded c-axis lattice constant. The comparison is based on the aligned sapphire (006) XRD peak.

3. DISCUSSION

Although we have only measured the phonon modes at large wave numbers, such as the E^1_{2g} and A_{1g}, when the lattice is under strain, the phonon modes at low wave numbers will also be modified. According to BCS theory,[21] the electron–phonon coupling strength is weakened when the stiffness of the lattice vibrations increases, which can be caused by a compressive strain. A similar effect was previously reported in other 2D materials such as MoS_2.[22] Our observations are in agreement with them and suggest that strain could cause the reduced T_c and the switching-off of superconductivity in $NbSe_2$ (Figure 3b inset). Interestingly, we only see lattice compression within the monolayer plane, whereas the c-axis is expanded (Figure 4c). Therefore, our results point out that the planar vibration modes play a more important role on superconductivity in $NbSe_2$.

According to SAD (Figure 4b) and RHEED (Figure 4b and Supporting Information Figure S2c) results, no structural phase differences are observed in between the superconducting and insulating samples. Previously, it was reported that 1T-$NbSe_2$ is a Mott insulator, which is obtained by growing $NbSe_2$ at a higher substrate temperature.[11] Our density functional theory (DFT) calculations show that the Raman activated modes are very different between 2H-$NbSe_2$ and 1T-$NbSe_2$ (Supporting Information Figure S4). Thus, our Raman results in Figure 4a do not suggest that our insulating sample is 1T-$NbSe_2$. We infer that the insulating behavior could be due to the modified electron correlations such as the charge density wave (CDW) or the change in band structure in $NbSe_2$ as a result of strain, which is often seen in TMD materials.[23]

Our results show that strain can serve as an effective knob in tuning the superconducting properties of $NbSe_2$, which, however, is hard to achieve by other means such as carrier density tuning.[24–26] The semiconducting (or insulating) $NbSe_2$ could serve as a high-quality tunnel barrier material with a good lattice match with the superconducting 2H-$NbSe_2$, thereby enabling a range of superconducting tunneling devices to be seamlessly built into $NbSe_2$. Further, the semiconducting (or insulating) $NbSe_2$ may allow gate-controlled insulator to superconductor transitions. TMD semiconductors in their 2H phase, for example, 2H-MoS_2, can become superconducting once a significant amount of charge carriers are injected into the material by gating.[27] Because our observed semiconducting (or insulating) $NbSe_2$ is in its 2H phase, superconductivity can potentially be turned on by a dielectric gate. It would thus enable switchable superconducting devices. These may also suggest the potential realization of 2D planar tunneling devices such as 2D Josephson junctions in $NbSe_2$, which has been predicted as a scalable platform for topological super-conductivity and the manipulation of Majorana zero modes for fault-tolerant topological quantum computing.[28]

4. CONCLUSION

The growth of few-layer $NbSe_2$ using MBE has the advantage of producing heterostructures with ultraclean interfaces, which are crucial for delivering high quality proximitized materials.[16] Because the grown $NbSe_2$ layers are very thin, the interface effect dominates the electrical properties of the hetero-structure. New phenomena due to various proximity effects, such as magnetic proximity effects, superconducting proximity effects, and spin–orbit proximity effects, can emerge. For magnetic proximity effect, heterostructures between NbSe2 and other materials with large magnetic exchange fields[29,30] can be grown in situ by MBE. The in situ growth enables ultraclean interface that is crucial for the induced exchange field, and such $NbSe_2$ heterostrucures are promising candidates for topological superconductors.[4–8] For spin–orbit proximity effect, heterostructures can be grown by combining $NbSe_2$ with other materials having strong spin–orbit coupling (SOC), for example TMD materials WTe_2, WSe_2, etc. $NbSe_2$ can acquire stronger SOC or an additional interface SOC, which can be further tuned by a dielectric gate thereby enabling new spintronic devices.

5. METHODS

Growth of the $NbSe_2$ thin films was carried out in an ultrahigh vacuum chamber with a base pressure of $\sim 3 \times 10^{-10}$ Torr. The films were monitored in situ throughout the growth by reflection high energy electron diffraction (RHEED) with a 7.5 mW beam energy. Ex situ Raman spectroscopy was carried out on uncapped films using a Horiba LabRam system. A 6 mW, 532 nm unpolarized excitation laser with a 100 μm spot size was used to scan the films. Ex situ X-ray diffraction was done using a PANalytical Empyrean Series 2 diffractometer with Cu K-Alpha1 line. Transport measurements were carried out in a homemade liquid helium probe. The sample was mounted inside the probe using pressed indium contacts, purged with He gas, and then cooled in a liquid helium dewar. Temperature was controlled by adjusting the insertion height of the probe. The temperatures below 4.2K were achieved by letting additional He gas condense inside the probe followed by pumping to reduce the vapor pressure. A Stanford Research Systems lock-in amplifier was used to measure the resistance of the films in a four-terminal configuration. The DFT calculations were carried out within the Perdew–Burke–Ernzerhof (PBE) generalized gradient approximation and the projected augmented wave (PAW) method as implemented in software package VASP.[31,32] The van der Waals (vdW) interactions were accounted for using Grimme's DFT-D2 semiempirical correction to the Kohn–Sham energies.[33]

■ ASSOCIATED CONTENT

ⓈI Supporting Information

The Supporting Information is available free of charge at https://pubs.acs.org/doi/10.1021/acsami.0c08804.

Sample growth (S1), sample characterization (S2), variable range hopping fitting to the insulating sample (S3), and DFT calculations of the phonon spectrum of 1T-$NbSe_2$ (S4) (PDF)

■ AUTHOR INFORMATION

Corresponding Author

Peng Wei — *Department of Physics and Astronomy, University of California, Riverside, California 92521, United States;* ⓞ orcid.org/0000-0003-2289-6007; Email: peng.wei@ucr.edu

Authors

Cliff Chen — *Department of Physics and Astronomy, University of California, Riverside, California 92521, United States*

Protik Das — *Department of Electrical and Computer Engineering, University of California, Riverside, California 92521, United States*

Ece Aytan — *Department of Electrical and Computer Engineering, University of California, Riverside, California 92521, United States*

Weimin Zhou — *Department of Physics and Astronomy, University of California, Riverside, California 92521, United States*

Justin Horowitz − *Department of Physics and Astronomy, University of California, Riverside, California 92521, United States*

Biswarup Satpati − *Surface Physics & Material Science Division, Saha Institute of Nuclear Physics, Bidhannagar, Kolkata 700 064, India*

Alexander A. Balandin − *Department of Electrical and Computer Engineering, University of California, Riverside, California 92521, United States*

Roger K. Lake − *Department of Electrical and Computer Engineering, University of California, Riverside, California 92521, United States;* ⓘ orcid.org/0000-0002-3318-7962

Complete contact information is available at:
https://pubs.acs.org/10.1021/acsami.0c08804

Notes
The authors declare no competing financial interest.

■ REFERENCES

(1) Xi, X.; Wang, Z.; Zhao, W.; Park, J.-H.; Law, K. T.; Berger, H.; Forro, L.; Shan, J.; Mak, K. F. Ising pairing in superconducting NbSe2 atomic layers. *Nat. Phys.* **2016**, *12*, 139−143.

(2) Xing, Y.; Zhao, K.; Shan, P.; Zheng, F.; Zhang, Y.; Fu, H.; Liu, Y.; Tian, M.; Xi, C.; Liu, H.; Feng, J.; Lin, X.; Ji, S.; Chen, X.; Xue, Q.-K.; Wang, J. Ising Superconductivity and Quantum Phase Transition in Macro-Size Monolayer NbSe2. *Nano Lett.* **2017**, *17*, 6802−6807.

(3) de la Barrera, S. C.; Sinko, M. R.; Gopalan, D. P.; Sivadas, N.; Seyler, K. L.; Watanabe, K.; Taniguchi, T.; Tsen, A. W.; Xu, X.; Xiao, D.; Hunt, B. M. Tuning Ising superconductivity with layer and spin−orbit coupling in two-dimensional transition-metal dichalcogenides. *Nat. Commun.* **2018**, *9*, 1427.

(4) Zhou, B. T.; Yuan, N. F. Q.; Jiang, H.-L.; Law, K. T. Ising superconductivity and Majorana fermions in transition-metal dichalcogenides. *Phys. Rev. B: Condens. Matter Mater. Phys.* **2016**, *93*, 180501.

(5) Triola, C.; Badiane, D. M.; Balatsky, A. V.; Rossi, E. General Conditions for Proximity-Induced Odd-Frequency Superconductivity in Two-Dimensional Electronic Systems. *Phys. Rev. Lett.* **2016**, *116*, 257001.

(6) Hsu, Y.-T.; Vaezi, A.; Fischer, M. H.; Kim, E.-A. Topological superconductivity in monolayer transition metal dichalcogenides. *Nat. Commun.* **2017**, *8*, 14985.

(7) Rahimi, M. A.; Moghaddam, A. G.; Dykstra, C.; Governale, M.; Zülicke, U. Unconventional superconductivity from magnetism in transition-metal dichalcogenides. *Phys. Rev. B: Condens. Matter Mater. Phys.* **2017**, *95*, 104515.

(8) He, W.-Y.; Zhou, B. T.; He, J. J.; Yuan, N. F. Q.; Zhang, T.; Law, K. T. Magnetic field driven nodal topological superconductivity in monolayer transition metal dichalcogenides. *Communications Physics* **2018**, *1*, 40.

(9) Xi, X.; Zhao, L.; Wang, Z.; Berger, H.; Forró, L.; Shan, J.; Mak, K. F. Strongly enhanced charge-density-wave order in monolayer NbSe2. *Nat. Nanotechnol.* **2015**, *10*, 765.

(10) Bischoff, F.; Auwärter, W.; Barth, J. V.; Schiffrin, A.; Fuhrer, M.; Weber, B. Nanoscale Phase Engineering of Niobium Diselenide. *Chem. Mater.* **2017**, *29*, 9907−9914.

(11) Nakata, Y.; Sugawara, K.; Shimizu, R.; Okada, Y.; Han, P.; Hitosugi, T.; Ueno, K.; Sato, T.; Takahashi, T. Monolayer 1T-NbSe2 as a Mott insulator. *NPG Asia Mater.* **2016**, *8*, No. e321.

(12) Ugeda, M. M.; Bradley, A. J.; Zhang, Y.; Onishi, S.; Chen, Y.; Ruan, W.; Ojeda-Aristizabal, C.; Ryu, H.; Edmonds, M. T.; Tsai, H.-Z.; Riss, A.; Mo, S.-K.; Lee, D.; Zettl, A.; Hussain, Z.; Shen, Z.-X.; Crommie, M. F. Characterization of collective ground states in single-layer NbSe2. *Nat. Phys.* **2016**, *12*, 92.

(13) Mattheiss, L. F. Band Structures of Transition-Metal-Dichalcogenide Layer Compounds. *Phys. Rev. B* **1973**, *8*, 3719−3740.

(14) Nakano, M.; Wang, Y.; Kashiwabara, Y.; Matsuoka, H.; Iwasa, Y. Layer-by-Layer Epitaxial Growth of Scalable WSe2 on Sapphire by Molecular Beam Epitaxy. *Nano Lett.* **2017**, *17*, 5595−5599.

(15) Moser, J.; Matos-Abiague, A.; Schuh, D.; Wegscheider, W.; Fabian, J.; Weiss, D. Tunneling Anisotropic Magnetoresistance and Spin-Orbit Coupling in Fe/GaAs/Au Tunnel Junctions. *Phys. Rev. Lett.* **2007**, *99*, 056601.

(16) Žutić, I.; Matos-Abiague, A.; Scharf, B.; Dery, H.; Belashchenko, K. Proximitized materials. *Mater. Today* **2019**, *22*, 85−107.

(17) Samnakay, R.; Wickramaratne, D.; Pope, T. R.; Lake, R. K.; Salguero, T. T.; Balandin, A. A. Zone-Folded Phonons and the Commensurate−Incommensurate Charge-Density-Wave Transition in 1T-TaSe2 Thin Films. *Nano Lett.* **2015**, *15*, 2965−2973.

(18) Aytan, E.; Debnath, B.; Kargar, F.; Barlas, Y.; Lacerda, M. M.; Li, J. X.; Lake, R. K.; Shi, J.; Balandin, A. A. Spin-phonon coupling in antiferromagnetic nickel oxide. *Appl. Phys. Lett.* **2017**, *111*, 252402.

(19) Pak, S.; Lee, J.; Lee, Y.-W.; Jang, A. R.; Ahn, S.; Ma, K. Y.; Cho, Y.; Hong, J.; Lee, S.; Jeong, H. Y.; Im, H.; Shin, H. S.; Morris, S. M.; Cha, S.; Sohn, J. I.; Kim, J. M. Strain-Mediated Interlayer Coupling Effects on the Excitonic Behaviors in an Epitaxially Grown MoS2/WS2 van der Waals Heterobilayer. *Nano Lett.* **2017**, *17*, 5634−5640.

(20) Pereira, C. M.; Liang, W. Y. Raman studies of the normal phase of 2H-NbSe 2. *J. Phys. C: Solid State Phys.* **1982**, *15*, L991.

(21) Bardeen, J.; Cooper, L. N.; Schrieffer, J. R. Theory of Superconductivity. *Phys. Rev.* **1957**, *108*, 1175−1204.

(22) Fu, Y.; Liu, E.; Yuan, H.; Tang, P.; Lian, B.; Xu, G.; Zeng, J.; Chen, Z.; Wang, Y.; Zhou, W.; Xu, K.; Gao, A.; Pan, C.; Wang, M.; Wang, B.; Zhang, S.-C.; Cui, Y.; Hwang, H. Y.; Miao, F. Gated tuned superconductivity and phonon softening in monolayer and bilayer MoS2. *npj Quantum Materials* **2017**, *2*, 52.

(23) Hui, Y. Y.; Liu, X.; Jie, W.; Chan, N. Y.; Hao, J.; Hsu, Y.-T.; Li, L.-J.; Guo, W.; Lau, S. P. Exceptional Tunability of Band Energy in a Compressively Strained Trilayer MoS2 Sheet. *ACS Nano* **2013**, *7*, 7126−7131.

(24) Staley, N. E.; Wu, J.; Eklund, P.; Liu, Y.; Li, L.; Xu, Z. Electric field effect on superconductivity in atomically thin flakes of NbSe2. *Phys. Rev. B: Condens. Matter Mater. Phys.* **2009**, *80*, 184505.

(25) El-Bana, M. S.; Wolverson, D.; Russo, S.; Balakrishnan, G.; Paul, D. M.; Bending, S. J. Superconductivity in two-dimensional NbSe2 field effect transistors. *Supercond. Sci. Technol.* **2013**, *26*, 125020.

(26) Xi, X.; Berger, H.; Forró, L.; Shan, J.; Mak, K. F. Gate Tuning of Electronic Phase Transitions in Two-Dimensional NbSe2. *Phys. Rev. Lett.* **2016**, *117*, 106801.

(27) Ye, J. T.; Zhang, Y. J.; Akashi, R.; Bahramy, M. S.; Arita, R.; Iwasa, Y. Superconducting Dome in a Gate-Tuned Band Insulator. *Science* **2012**, *338*, 1193.

(28) Zhou, T.; Dartiailh, M. C.; Mayer, W.; Han, J. E.; Matos-Abiague, A.; Shabani, J.; Žutić, I. Phase Control of Majorana Bound States in a Topological X Junction. *Phys. Rev. Lett.* **2020**, *124*, 137001.

(29) Wang, Z.; Tang, C.; Sachs, R.; Barlas, Y.; Shi, J. Proximity-Induced Ferromagnetism in Graphene Revealed by the Anomalous Hall Effect. *Phys. Rev. Lett.* **2015**, *114*, 016603.

(30) Wei, P.; Lee, S.; Lemaitre, F.; Pinel, L.; Cutaia, D.; Cha, W.; Katmis, F.; Zhu, Y.; Heiman, D.; Hone, J.; Moodera, J. S.; Chen, C.-T. Strong interfacial exchange field in the graphene/EuS heterostructure. *Nat. Mater.* **2016**, *15*, 711.

(31) Perdew, J. P.; Burke, K.; Ernzerhof, M. Generalized Gradient Approximation Made Simple. *Phys. Rev. Lett.* **1996**, *77*, 3865−3868.

(32) Kresse, G.; Joubert, D. From ultrasoft pseudopotentials to the projector augmented-wave method. *Phys. Rev. B: Condens. Matter Mater. Phys.* **1999**, *59*, 1758−1775.

(33) Grimme, S. Semiempirical GGA-type density functional constructed with a long-range dispersion correction. *J. Comput. Chem.* **2006**, *27*, 1787−1799.

(34) Towns, J.; Cockerill, T.; Dahan, M.; Foster, I.; Gaither, K.; Grimshaw, A.; Hazlewood, V.; Lathrop, S.; Lifka, D.; Peterson, G. D.; Roskies, R.; Scott, J. R.; Wilkins-Diehr, N. XSEDE: Accelerating Scientific Discovery. *Comput. Sci. Eng.* **2014**, *16*, 62−74.